NASA TECHNICAL MEMORANDUM

NASA TM X-1136

NASA TM X-1136

COMPARISON OF MEASURED AND CALCULATED TURBULENT HEAT TRANSFER IN A UNIFORM AND NONUNIFORM FLOW FIELD ON THE X-15 UPPER VERTICAL FIN AT MACH NUMBERS OF 4.2 AND 5.3

by Ronald P. Banas

Flight Research Center
Edwards, Calif.

NATIONAL AERONAUTICS AND SPACE ADMINISTRATION • WASHINGTON, D. C. • SEPTEMBER 1965

NASA TM X-1136

COMPARISON OF MEASURED AND CALCULATED TURBULENT HEAT TRANSFER IN A UNIFORM AND NONUNIFORM FLOW FIELD ON THE X-15 UPPER VERTICAL FIN AT MACH NUMBERS OF 4.2 AND 5.3

By Ronald P. Banas

Flight Research Center
Edwards, Calif.

NATIONAL AERONAUTICS AND SPACE ADMINISTRATION

COMPARISON OF MEASURED AND CALCULATED TURBULENT HEAT TRANSFER IN A UNIFORM AND NONUNIFORM FLOW FIELD ON THE X-15 UPPER VERTICAL FIN AT MACH NUMBERS OF 4.2 AND 5.3*

By Ronald P. Banas
Flight Research Center

SUMMARY

Turbulent heat-transfer coefficients and measured local static pressures were obtained in flight on the X-15 upper vertical fin with both a sharp and a blunt leading edge. The data are compared with calculated values. Calculated and measured Mach number profiles in the shear layer are also presented.

Heat-transfer coefficients were obtained from measured skin temperatures at free-stream Mach numbers of approximately 4.2 and 5.3 and free-stream Reynolds numbers between 1.8×10^6 and 2.5×10^6 per foot. Comparisons of measured and calculated heat-transfer coefficients obtained in both a uniform flow field and a nonuniform flow field show that the heat-transfer coefficients calculated by Eckert's reference-temperature method were from 32 percent to 57 percent higher than the measured values.

INTRODUCTION

The X-15 flight-research program has included many flights to investigate the effects of aerodynamic heating and to determine the adequacy of the heat-transfer methods used in the design of the X-15.

Early heat-transfer results on the X-15 at Mach numbers of 3, 4, and 5 and at low angles of attack (ref. 1) indicated that the reference-temperature method of Eckert (ref. 2) for turbulent flow overestimated the measured heat-transfer coefficients by as much as 60 percent. Reference 1 also showed that closer agreement was obtained when the effect of heating rate on the reference temperature was neglected (the adiabatic-wall reference-temperature method). Reference 3 compared the methods of Van Driest (ref. 4), Eckert (ref. 2), and reference 1 in temperature time-history form to X-15 data at Mach numbers of 4, 5, and 6. The study concluded that the method of Eckert, with the effect of heating rate neglected, estimated the measured temperatures at various locations on the X-15 with sufficient accuracy for flight-safety purposes. The close agreement between measured and calculated heat transfer (ref. 1) and skin temperature (ref. 3) was obtained by assuming attached-shock (uniform) flow conditions and neglecting the effect of heating rate.

*Title, Unclassified.

Since the measured data were obtained in the presence of a shear (entropy) layer[1] that extends well past the boundary-layer edge, Quinn and Kuhl in a subsequent paper (ref. 6) used calculated shear layers to determine flow conditions at the outer edge of the boundary layer in their analysis of the measured heat-transfer data. They concluded that, with the shear layer taken into account, the theories of Van Driest and Eckert still overestimated the heat transfer on the fuselage by 35 percent to 60 percent and on the wing by 30 percent to 45 percent.

In order to minimize the uncertainties in the analysis of the measured heat-transfer data associated with the bluntness-induced flow conditions, the upper fin of the X-15 was modified to incorporate a sharp-leading-edge configuration. Data were obtained on both the original blunt-leading-edge fin and the modified sharp-leading-edge fin. This paper discusses the flow conditions and presents measurements of heat transfer in a uniform flow field (attached shock) and in a nonuniform flow field (detached shock) at the instrumented chord of the upper fin. In addition, heat-transfer data from the wing and fuselage of the X-15 are included for comparison with the fin data. The measured heat-transfer data are compared with the method of Eckert, and the flow-field data are compared with the method of Moeckel.

SYMBOLS

$A = \rho_w b_w c_{p,w}$

b_w skin thickness, ft

c_p specific heat of air, $\frac{\text{Btu}}{\text{lb-}^\circ\text{F}}$

$c_{p,w}$ specific heat of skin material, $\frac{\text{Btu}}{\text{lb-}^\circ\text{F}}$ (linear variation for Inconel X from 0.11 at 200° F to 0.14 at 1300° F, ref. 7)

H altitude, ft

h heat-transfer coefficient, $\frac{\text{Btu}}{\text{ft}^2\text{-}^\circ\text{F-sec}}$

M Mach number

Pr Prandtl number

p absolute static pressure, lb/ft^2

---

[1]A flow field with a Mach number gradient, normal to the flow direction, produced by the normal and highly curved portion of the detached shock wave associated with a blunt leading edge (ref. 5).

Re Reynolds number, $\frac{\rho V x}{\mu}$

St Stanton number, $\frac{h}{\rho_l V_l c_{p,l}}$

T_r recovery temperature, °R

T_w skin temperature, °R

t time, sec

V velocity, ft/sec

x flow length measured from leading edge, ft

y height above surface, in.

$Z = A\frac{dT_w}{dt} + \sigma\epsilon {T_w}^4$

α angle of attack, deg

β angle of sideslip, deg

Δ error (appendix only)

δ angle of deflection of upper vertical fin, deg

ϵ emissivity of skin material, 0.76

μ dynamic viscosity, lb/ft-sec

ρ density of air, lb/ft^3

ρ_w density of skin material (for Inconel X, 515 lb/ft^3)

σ Stefan-Boltzmann constant, 4.78×10^{-13} $\frac{\text{Btu}}{\text{ft}^2\text{-sec-°R}^4}$, and standard deviation (appendix only)

Subscripts:

av average

i incompressible

l local

∞ free stream

TEST SURFACE

The general test area of this investigation is shown on the three-view drawing of the X-15 in figure 1.

To generate a uniform flow field, the leading edge of the movable upper vertical fin of the X-15 was changed from a blunt, 1.0-inch-diameter, 5° half-angle wedge to a sharp, 0.030-inch-diameter, 5° half-angle wedge. The new leading edge, machined from type 347 stainless steel, increased the chord length 5 inches. Figure 2 shows the fixed and movable portions of the fin, detailed section views of the sharp and the blunt leading-edge configurations, and pertinent dimensions.

To insure turbulent flow along the fin, boundary-layer trips consisting of spot welds 0.125 inch in diameter and 0.020 inch to 0.025 inch high were placed along the right side of the fin 5 inches from the leading edge (fig. 2). Figure 3 shows a closeup view of the sharp leading edge and a boundary-layer trip. Additional information on the vertical fin and other physical characteristics of the X-15 is included in reference 3.

INSTRUMENTATION

A shear-layer rake was mounted on the left side of the sharp fin 27 inches from the leading edge and 12 inches from the top of the fin. Figure 4(a) shows the shear-layer rake in the location at which the uniform flow-field data were obtained. Figure 4(b) shows the shear-layer rake fastened to the blunt fin at the 93-percent-chord position, the location at which the nonuniform data were obtained.

The locations of surface thermocouples and static-pressure orifices on the upper vertical fin are shown in figure 2. The thermocouples were fastened to both the right and the left sides of the vertical fin; whereas, the static-pressure orifices were placed on the right side only. The skin thickness at the thermocouple locations, flow distance from the leading edge, and percent chord corresponding to the flow distance are presented in table I for both the blunt and the sharp fin. Other pertinent dimensions for the blunt fin are listed in table II.

The thermocouples were 30-gage chromel-alumel wires spot-welded to the inside surface of the skin. The static-pressure orifices were 0.250-inch inner-diameter tubing installed flush with the outside surface of the skin. The entire shear-layer rake was constructed of Inconel X. The surface orifices and impact probes were connected by tubing to standard NACA self-recording mechanical-optical manometers in the side fairing of the fuselage.

The lag in the static-pressure system was determined from the data of reference 8 to be negligible for the flight conditions at which the heat-transfer coefficients were obtained, and the static-pressure measurements are accurate to ±10 lb/ft^2 (ref. 9). Since the impact pressure is much greater than the static pressure, the lag in the impact-pressure system was assumed to be negligible. The resulting error in local Mach number arising from combining the impact- and static-pressure errors is ±0.1.

The overall accuracy of the thermocouple system is ±15° F. By using the measured skin temperature and assuming a limit error of ±15° F, the resulting probable error in heating rate is ±0.844 deg/sec. The errors in the heat-transfer coefficients, as derived from measured data, are analyzed in the appendix.

TEST CONDITIONS

Heat-transfer coefficients were derived from measured skin temperatures during quasi-steady periods of four X-15 flights--two with the sharp-leading-edge vertical fin (3-23 and 3-31)[1], and two with the blunt leading edge (2-22 and 2-29). A typical flight time history (3-23) is shown in figure 5. The shaded area typifies the quasi-steady periods in which velocity, altitude, angle of attack, and angle of sideslip were changing slowly in comparison with the other portions of the flight. The free-stream Mach number, static pressure, static temperature, angle of attack, angle of sideslip, upper-fin deflection, and measured skin temperature for the quasi-steady periods of each flight are listed in tables III and IV, and the measured surface pressures for the various chord positions are listed in tables V and VI. Heat-transfer coefficients were derived at the following conditions:

	Sharp leading edge		Blunt leading edge	
Flight	3-23	3-31	2-22	2-29
t, sec	80	87	90	116
M_∞	4.28	5.31	5.27	4.19
Re_∞ per foot	2.42×10^6	1.86×10^6	2.40×10^6	2.45×10^6

DATA REDUCTION

The following equation for thin-skin heat balance was used to derive the heat-transfer coefficients from the measured skin temperatures

$$h = \frac{\rho_w c_{p,w} b_w \frac{dT_w}{dt} + \sigma \epsilon T_w^4}{(T_r - T_w)} \tag{1}$$

[1] In the flight-designation system used for the X-15, the first digit is the airplane number; the following digits indicate the free-flight number.

The skin temperatures T_w were recorded at 1-second intervals. To determine the heating rates $\frac{dT_w}{dt}$, nine data points were fitted with a second-order curve. The derivative at the midpoint was used to determine the heat-transfer coefficient. The turbulent recovery temperature T_r was calculated by using a recovery factor equal to the cube root of the Prandtl number evaluated at the reference temperature. The values of the recovery factor ranged from 0.90 to 0.91.

RESULTS AND DISCUSSION

Shear-Layer Measurements

The effects of the blunt and the sharp leading edges on the local-flow conditions were determined from shear-layer-rake measurements on the fin surface (fig. 4) during flights similar to those from which data were obtained for this investigation. Local Mach numbers were derived from the Rayleigh pitot-tube formula (ref. 10) by using measured pressures from the shear-layer-rake impact probes and surface orifices. The usual assumption of constant static pressure through the boundary layer was extended to the farthest impact-pressure probe (4.5 inches). The measured Mach number profiles for both the blunt and the sharp leading edges are shown in figures 6 and 7, respectively, for free-stream Mach numbers corresponding to those for which heat-transfer data are presented. The measured Mach number profiles are compared to those calculated for inviscid flow by the method of Moeckel (ref. 11), wherein the shock-wave shape computed by the method of Love (ref. 12) was used. This procedure is described in reference 6.

Blunt leading edge.– Calculated and measured Mach number profiles normal to the surface of the blunt-leading-edge fin are presented for $M_\infty = 4.2$ in figure 6(a) and for $M_\infty = 5.1$ in figure 6(b). The data show good agreement. The repeatability in the measurements can be seen in figure 6(b), in which data from two flights are presented.

About 1 inch above the surface, the measured local Mach numbers deviate from those based on inviscid-flow calculations. This deviation is caused by the presence of the boundary layer. Unpublished data from a boundary-layer rake at the 70-percent chord and the same span position as the shear-layer rake agreed well with boundary-layer thicknesses calculated by the method of references 13 and 14. At the shear-layer rake, the edge of the boundary layer was calculated to be 1 inch from the surface, as shown in the figure. If the Mach number at the outer edge of the boundary layer is assumed to be that given by the Moeckel-Love method 1 inch above the surface, the Mach number is less than 8.5 percent above the value calculated at the surface. This condition is seen by comparing the difference between the calculated local Mach numbers at $y = 0$ and $y = 1$ inch. Since the shear-layer profile is a function of the shock shape and, therefore, remains unchanged with flow distance for a constant pressure ratio $\frac{p_l}{p_\infty}$, the difference between the Mach number at the outer edge of the boundary layer and at the fin surface becomes even less as the boundary-layer height diminishes forward of the rake position. The effect of this small difference is insignificant in the calculation of the heat-transfer coefficients; therefore, the calculated inviscid surface values were used. The surface Mach number is easily calculated by using a swept-normal-shock procedure.[1]

Sharp leading edge.— Calculated and measured Mach number profiles are presented for $M_\infty = 4.2$ in figure 7(a) and for $M_\infty = 5.1$ in figure 7(b), the same free-stream Mach numbers as those at which the blunt-leading-edge data were obtained. Good agreement between the measured and the calculated data is shown. Again, data from two flights are presented, indicating good repeatability.

The calculations show that the local Mach number increases rapidly from the swept-normal-shock values[1] at the surface to the oblique-shock values near $y = 0.35$ inch. The Mach numbers measured at $y = 0.5$ inch indicate that the innermost probe is at or within the boundary-layer edge. This observation is supported by estimated boundary-layer heights of about 0.5 inch at this location. When these data are compared with those of figure 6, it may be seen that the shear layer produced by the installation of the sharp leading edge is reduced to the extent that the growth of the boundary layer takes place in essentially uniform flow. Accordingly, the boundary-layer-edge Mach numbers for the analysis of the sharp-fin heat-transfer data were calculated by using oblique-shock assumptions (ref. 15).

If the measured Mach numbers (above 0.5 inch) and the wedge half-angle are used with the Prandtl equation for an oblique shock (ref. 16, page 86), the resulting Mach number upstream of the vertical fin is within ±0.1 of the free-stream value. Hence, even in the highly complex flow field approaching the upper vertical fin of the X-15, the simple oblique-shock method adequately predicts the local conditions at the edge of the boundary layer.

Surface Pressures

Measured surface pressures on both fins are shown in figure 8 for the time in each flight at which heat-transfer coefficients are presented. The measured data are compared to calculated oblique-shock values at $M_\infty = 4.2$

---

[1]As applied in reference 6, a swept-normal-shock total pressure is computed by taking the component of the free-stream Mach number normal to the leading edge, and using this Mach number to obtain the total-pressure ratio across the shock wave from the normal-shock tables of reference 15. This total-pressure ratio is multiplied by the free-stream total pressure to obtain a swept-normal-shock total pressure behind the shock wave. The latter pressure is used with the measured static pressure to obtain the local Mach number that would exist at the surface in the absence of a boundary layer.

(fig. 8(a)) and $M_\infty = 5.3$ (fig. 8(b)). Except for the lower pressures measured at $x = 5$ feet and $x = 6.3$ feet on the sharp fin, the calculated values are in good agreement with the measurements. Accordingly, the oblique-shock assumption was considered adequate for calculating values of local static pressure at the boundary-layer edge. The lower pressures measured at $x = 5$ feet and $x = 6.3$ feet on the sharp fin are, as yet, unexplained; however, it may be noted that the effect is not discernible in the measured heat-transfer data of figure 9.

Other boundary-layer-edge conditions (density, velocity, and static temperature) were derived from isentropic-flow relationships, and the viscosity was evaluated by using Sutherland's equation (ref. 15).

Heat Transfer

Vertical-fin data.— Measured and calculated heat-transfer coefficients on both the blunt and the sharp fin are presented in figure 9 for free-stream Mach numbers of 4.2 and 5.3. The data were corrected for conduction losses at the thermocouple locations, as explained in the appendix. At $M_\infty = 4.2$ (fig. 9(a)), the conduction correction increased the value of the heat-transfer coefficient derived from equation (1) by 5.7 percent to 14.4 percent. At $M_\infty = 5.3$ (fig. 9(b)), the values were increased 5.9 percent to 10 percent (see table in appendix, page 16). In general, the differences between the data obtained on the left and the right sides of the fin are consistent with the estimated root-mean-square errors of about 7 percent for the data at $M_\infty = 5.3$ and 11 and 13 percent for the data at $M_\infty = 4.2$ (see appendix).

Differences between data from the left and the right sides have been noted only at the two most forward locations of the sharp fin where the data from the left side have shown consistently higher heat transfer than the data from the right side. Also, on the blunt fin at $x = 5$ feet, the data from both the right and the left sides have been consistently higher than the general level of the data forward and rearward of this location.

The measured data were faired for comparison with the calculated values obtained from the method of Eckert (ref. 2). This fairing is shown by the solid lines in figure 9. No significant differences, other than the exceptions noted previously, are evident in the comparison of the sharp- and the blunt-fin data for the range of flow lengths and Mach numbers investigated.

As shown in figure 9(a), the method of reference 2 overestimates the average value of the heat-transfer coefficients measured on the blunt fin by 34 percent to 48 percent and on the sharp fin by 38 percent to 42 percent. In figure 9(b) the calculated values are excessive by 41 percent to 57 percent for the blunt fin and by 32 percent to 42 percent for the sharp fin. Hence, whether the comparison is made in a uniform (sharp fin) or nonuniform (blunt fin) flow field, Eckert's method results in an overprediction of the measured heat-transfer coefficients.

Comparison of vertical-fin, wing, and fuselage data.— The trend to lower measured heat transfer than would be predicted by the method of Eckert was also observed in the data from the lower wing and fuselage (refs. 1 and 6). In figure 10, the wing and fuselage data of figures 10(b) and 11 of reference 6 are compared with blunt- and sharp-vertical-fin data in the form of compressible Stanton number (dimensionless heat-transfer coefficient) divided by the incompressible Stanton number as a function of local Mach number. In addition to the data of figure 9, blunt- and sharp-fin data from flights not reported herein are included. The measured compressible Stanton numbers were obtained by using the measured heat-transfer coefficients and calculated local-flow conditions. The flow conditions were calculated by using the attached-shock method for the sharp fin and the detached-shock method (see footnote, page 7) for the blunt fin. The incompressible Stanton numbers were calculated from the equation (ref. 6, appendix B)

$$St_i = \frac{0.0296}{(Re_l)^{1/5}(Pr_l)^{2/3}} \tag{2}$$

which was obtained by using Colburn's modified Reynolds analogy together with Blasius' relation for the flat-plate turbulent skin-friction coefficient.

The solid line in figure 10 represents the calculated Stanton number predicted by Eckert's method with the effect of heating rate neglected (the adiabatic-wall reference-temperature method). The following equation (ref. 6, eq. (B9)) was used in the calculation

$$\frac{St}{St_i} = \left(\frac{1}{1 + 0.1296M_l^2}\right)^{0.65} \tag{3}$$

The comparison shows the measured data to be in fair agreement with calculated results. It is particularly significant that, even in a uniform flow field (sharp fin), the level of the heat-transfer data is about the same as reported in reference 6. Also, the fact that the adiabatic-wall reference-temperature method gives a better estimate of the heat transfer than the method of Eckert is demonstrated generally for all Mach numbers and test locations on the X-15.

CONCLUSIONS

Comparison of measured and calculated turbulent heat-transfer coefficients on the X-15 shows that:

1. The method of Moeckel and Love provided a good approximation to the measured shear-layer profile at free-stream Mach numbers of 4.2 and 5.1 on both the blunt-leading-edge and the sharp-leading-edge vertical fin.

2. Turbulent heat-transfer coefficients predicted by Eckert's method, based on measured values of the local-flow conditions on the sharp-leading-edge fin, overestimated the measured heat transfer by 32 percent to 42 percent.

3. Turbulent heat-transfer coefficients predicted by Eckert's method, based on measured local-flow conditions on the blunt-leading-edge fin, overestimated the measured heat transfer by 34 percent to 57 percent.

4. The levels of turbulent heat transfer measured on the blunt- and the sharp-leading-edge vertical fin compare favorably with previously reported data on the wing and fuselage; the levels were near the values given by Eckert's reference-temperature method when the adiabatic-wall temperature was used in lieu of the actual skin temperature to calculate the reference temperature.

Flight Research Center,
National Aeronautics and Space Administration,
Edwards, Calif., May 28, 1965.

APPENDIX

ERROR ANALYSIS

The probable error in the measured heat-transfer coefficients derived from equation (1) was estimated by using the concept of a limit error.[1] In combination with a Gaussian distribution, the probable error (see ref. 17) is equal to 0.675 times the standard deviation σ and represents the deviation for which the probability of being exceeded is one-half. After the total differential of equation (1) was divided by equation (1), the probable error for each of the significant quantities was combined as an independent error (ref. 18) according to the following equation

$$\left(\frac{\Delta h}{h}\right)^2 = \left(\frac{A\frac{dT_w}{dt}}{Z}\right)^2\left(\frac{\Delta b_w}{b_w}\right)^2 + \left(\frac{A\frac{dT_w}{dt}}{Z}\right)^2\left(\frac{\Delta\frac{dT_w}{dt}}{\frac{dT_w}{dt}}\right)^2 + \left[\frac{ZT_w + (4)(T_r - T_w)\left(\sigma\epsilon T_w^{\ 4}\right)}{Z(T_r - T_w)}\right]^2\left(\frac{\Delta T_w}{T_w}\right)^2$$

$$+ \left(\frac{T_r}{T_r - T_w}\right)^2\left(\frac{\Delta T_\infty}{T_\infty}\right)^2 + \left[\frac{2(T_r - T_\infty)}{T_r - T_w}\right]^2\left(\frac{\Delta M_\infty}{M_\infty}\right)^2 + \left(\frac{\epsilon\sigma T_w^{\ 4}}{Z}\right)^2\left(\frac{\Delta\epsilon}{\epsilon}\right)^2 \qquad \text{(A1)}$$

where

$$A = \rho_w b_w c_{p,w}$$

$$Z = A\frac{dT_w}{dt} + \sigma\epsilon T_w^{\ 4}$$

$$T_r = \left[1 + 0.2(Pr_l)^{1/3}M_l^{\ 2}\right]T_l \approx \left[1 + 0.2(Pr_\infty)^{1/3}M_\infty^{\ 2}\right]T_\infty$$

To obtain values of the slope of wall temperature $\frac{dT_w}{dt}$ the least-squares method was first used to fit a second-order curve through nine values of the measured wall temperature. This fitted curve was then differentiated at its midpoint to obtain $\frac{dT_w}{dt}$. This slope was used as the average value $\left(\frac{dT_w}{dt}\right)_{av}$ and was also the value used to determine the heat-transfer coefficients in figure 9. The end points of the nine values of wall temperature were then adjusted by ±15° F to account for the overall limit error in the thermocouple system. These adjusted end points, along with the original center point, were used to determine derivatives at the midpoint that would represent

---

[1] The maximum amount by which the quantity may reasonably be supposed to be in error, sometimes designated as 3σ.

the limit maximum and the limit minimum deviation from the average slope $\left(\frac{dT_w}{dt}\right)_{av}$.

The difference between the limit maximum slope and the average slope was assumed to equal three standard deviations in the Gaussian distribution. The probable error of 0.675 of a standard deviation was then determined and used in equation (A1) along with the other similarly obtained values listed in the following table:

Quantity	Limit error (3σ)	Probable error (0.675σ)
$\frac{dT_w}{dt}$	±3.75 deg/sec	[a]±0.844 deg/sec
b_w	[b]±0.00042 ft	±0.000093 ft
T_w	±15° F	±4° F
T_∞	-------------	[c]±4° F
V_∞	-------------	±50 fps
M_∞	-------------	[d]±0.0517
ϵ	-------------	±0.038

[a]Constant error for a nine-point curve fit.
[b]X-15 manufacturer's drawings.
[c]Reference 19.
[d]Estimated.

Example Calculations

In order to show the magnitude of the statistical root-mean-square error in the heat-transfer coefficient, three example calculations representative of the data from the four flights shown in figure 9 have been made by using equation (A1).

From the following examples, it will be seen that the data with the smallest statistical root-mean-square error are obtained at the higher heating rates. The analysis will show that the heating-rate error, in the second term of equation (A1), outweighs the other possible errors in most instances. The other errors also contribute heavily to the low-heating-rate data (example 3) in such a manner as to yield a large statistical root-mean-square error.

Example 1.— For flights 3-31 and 2-22 with the sharp and the blunt fin, the following conditions were used:

$$M_\infty = 5.3$$

$$x = 2.57 \text{ ft}$$

$$\rho_w = 515 \text{ lb/cu ft}$$

$$b_w = 0.00308 \text{ ft}$$

$$c_{p,w} = 0.127 \frac{\text{Btu}}{\text{lb-}^\circ\text{F}}$$

$$A = \rho_w b_w c_{p,w} = (515)(0.00308)(0.127) = 0.2014 \frac{\text{Btu}}{\text{ft}^2\text{-}^\circ\text{F}}$$

The slope $\frac{dT_w}{dt}$ was obtained as discussed previously at $t = 90$ seconds for flight 2-22 and at $t = 87$ seconds for flight 3-31. The following typical value was used for both flights

$$\frac{dT_w}{dt} = 13.7^\circ \text{ F per sec at } T_w = 1{,}275^\circ \text{ R}$$

Thus

$$Z = \rho_w b_w c_{p,w} \frac{dT_w}{dt} + \sigma\epsilon T_w^4$$

$$Z = 3.719$$

The recovery temperature, as determined from enthalpy considerations, yields $T_r = 2{,}290^\circ$ R and $T_\infty = 381^\circ$ R.

Substitution of the values of Z, A, T_w, T_r, and T_∞ along with the values of the probable error from the preceding table into equation (A1) gives

$$\left(\frac{\Delta h}{h}\right)^2 = 5.042 \times 10^{-4} + 20.842 \times 10^{-4} + 0.515 \times 10^{-4} + 5.611 \times 10^{-4}$$
$$+ 13.464 \times 10^{-4} + 1.666 \times 10^{-4}$$

$$\frac{\Delta h}{h} = \pm 0.069 \text{ or } \pm 6.9 \text{ percent}$$

Hence, the probable root-mean-square error in the heat-transfer coefficient for flights 3-31 and 2-22 (fig. 9) was ±6.9 percent.

Example 2.- For flight 3-23 with the sharp fin, the following conditions were used:

$$M_\infty = 4.23$$

$$x = 2.576 \text{ ft}$$

$$\rho_w = 515 \text{ lb/cu ft}$$

$$b_w = 0.00308 \text{ ft}$$

$$c_{p,w} = 0.122 \frac{\text{Btu}}{\text{lb-}°\text{F}}$$

$$A = \rho_w b_w c_{p,w} = (515)(0.00308)(0.122) = 0.1935 \frac{\text{Btu}}{\text{ft}^2\text{-}°\text{F}}$$

The slope $\frac{dT_w}{dt}$, as obtained for $t = 80$ seconds, was

$$\frac{dT_w}{dt} = 8.10° \text{ F per sec for } T_w = 1{,}105° \text{ R}$$

Thus

$$Z = \rho_w b_w c_{p,w} \frac{dT_w}{dt} + \sigma\epsilon T_w{}^4$$

$$Z = 2.109$$

Using $T_r = 1{,}582°$ R and $T_\infty = 384°$ R and substituting the values of Z, A, T_w, T_r, and T_∞ along with the values of the probable error from the preceding table into equation (A1) gives

$$\left(\frac{\Delta h}{h}\right)^2 = 5.071 \times 10^{-4} + 59.965 \times 10^{-4} + 1.465 \times 10^{-4} + 11.934 \times 10^{-4}$$
$$+ 36.158 \times 10^{-4} + 1.649 \times 10^{-4}$$

$$\frac{\Delta h}{h} = \pm 0.106 \text{ or } \pm 10.6 \text{ percent}$$

Hence, the probable root-mean-square error in the heat-transfer coefficient for flight 3-23 was ±10.6 percent.

Example 3.— For flight 2-29 with the blunt fin, the following conditions were used:

$$M_\infty = 4.2$$

$$x = 2.57 \text{ ft}$$

$$\rho_w = 515 \text{ lb/cu ft}$$

$$b_w = 0.00308 \text{ ft}$$

$$c_{p,w} = 0.122 \frac{\text{Btu}}{\text{lb-}^\circ\text{F}}$$

$$A = \rho_w b_w c_{p,w} = (515)(0.00308)(0.122) = 0.1935 \frac{\text{Btu}}{\text{ft}^2\text{-}^\circ\text{F}}$$

The slope $\frac{dT_w}{dt}$ was obtained for $t = 116$ seconds, yielding

$$\frac{dT_w}{dt} = 4.93^\circ \text{ F per sec for } T_w = 1{,}122^\circ \text{ R}$$

Thus

$$Z = \rho_w b_w c_{p,w} \frac{dT_w}{dt} + \sigma\epsilon T_w^{\,4}$$

$$Z = 1.530$$

Using $T_r = 1{,}568^\circ$ R and $T_\infty = 383^\circ$ R and substituting the values of Z, A, T_w, T_r, and T_∞ along with the values of the probable error from the preceding table into equation (A1) results in

$$\left(\frac{\Delta h}{h}\right)^2 = 3.572 \times 10^{-4} + 114.001 \times 10^{-4} + 2.055 \times 10^{-4} + 13.482 \times 10^{-4} + 42.799 \times 10^{-4} + 3.541 \times 10^{-4}$$

$$\frac{\Delta h}{h} = \pm 0.134 \text{ or } \pm 13.4 \text{ percent}$$

Conduction Errors

A significant quantity, not included in the preceding error analysis, is the effect of internal conduction. Because of its tendency to be in one direction (to reduce the measured heat-transfer coefficient), this effect was considered separately. Since the vertical fin of the X-15 includes various spars and ribs, the effect of these structural elements as heat sinks was considered in a digital-computer program (thermal analyzer) that solves the transient heat-conduction equation.

By assuming that the thermocouples were placed midway between the rib centerlines, the internal conduction losses were determined for the times at which heat-transfer coefficients are shown in figure 9. The percentage increase in heat-transfer coefficient shown in the following table is the average value for the thermocouples between the indicated positions:

Condition	Thermocouple position, ft	Average increase in h, percent
$M = 4.2$		
Blunt fin Flight 2-29 $t = 116$ sec	1.29 to 1.71 2.14 to 7.78	14.4 7.5
Sharp fin Flight 3-23 $t = 80$ sec	1.719 to 2.147 2.576 to 8.212	11.3 5.7
$M = 5.3$		
Blunt fin Flight 2-22 $t = 90$ sec	1.29 to 1.71 2.14 to 7.78	10.0 6.0
Sharp fin Flight 3-31 $t = 87$ sec	1.719 to 2.147 2.576 to 8.212	8.9 5.9

REFERENCES

1. Banner, Richard D.; Kuhl, Albert E.; and Quinn, Robert D.: Preliminary Results of Aerodynamic Heating Studies on the X-15 Airplane. NASA TM X-638, 1962.

2. Eckert, Ernst R. G.: Survey on Heat Transfer at High Speeds. WADC Tech. Rep. 54-70 (Contract No. AF 33(616)-2214, RDO No. 474-143), Wright Air Dev. Center, U.S. Air Force, Apr. 1954.

3. Watts, Joe D.; and Banas, Ronald P.: X-15 Structural Temperature Measurements and Calculations for Flights to Maximum Mach Numbers of Approximately 4, 5, and 6. NASA TM X-883, 1963.

4. van Driest, E. R.: The Problem of Aerodynamic Heating. Aero. Eng. Rev., vol. 15, no. 10, Oct. 1956, pp. 26-41.

5. Yakura, James K.: Theory of Entropy Layers and Nose Bluntness in Hypersonic Flow. Vol. 7 of Progress in Astronautics and Rocketry, div. C, F. R. Riddell, ed., Academic Press, Inc., 1962, pp. 422-423.

6. Quinn, Robert D.; and Kuhl, Albert E.: Comparison of Flight-Measured and Calculated Turbulent Heat Transfer on the X-15 Airplane at Mach Numbers From 2.5 to 6.0 at Low Angles of Attack. NASA TM X-939, 1964.

7. Sachs, G.; and Pray, R. Ford, III, eds.: Air Weapons Materials Application Handbook. Metals and Alloys. First ed., TR 59-66 (ASTIA No. AD 252301), USAF Air Res. and Develop. Command, Dec. 1959.

8. Saltzman, Edwin J.: Base Pressure Coefficients Obtained From the X-15 Airplane for Mach Numbers Up to 6. NASA TN D-2420, 1964.

9. Pyle, Jon S.: Flight-Measured Wing Surface Pressures and Loads for the X-15 Airplane at Mach Numbers From 1.2 to 6.0. NASA TN D-2602, 1965.

10. Shapiro, Ascher H.: The Dynamics and Thermodynamics of Compressible Fluid Flow. Vol. I. The Ronald Press Co. (New York), c.1953, p. 153.

11. Moeckel, W. E.: Some Effects of Bluntness on Boundary-Layer Transition and Heat Transfer at Supersonic Speeds. NACA Rept. 1312, 1957. (Supersedes NACA TN 3653.)

12. Love, Eugene S.: A Reexamination of the Use of Simple Concepts for Predicting the Shape and Location of Detached Shock Waves. NACA TN 4170, 1957.

13. Reshotko, Eli; and Tucker, Maurice: Approximate Calculation of the Compressible Turbulent Boundary Layer With Heat Transfer and Arbitrary Pressure Gradient. NACA TN 4154, 1957.

14. Persh, Jerome; and Lee, Roland: Tabulation of Compressible Turbulent Boundary Layer Parameters. NAVORD Rept. 4282 (Aeroballistic Res. Rept. 337), U.S. Naval Ordnance Laboratory, White Oak, Md., May 1, 1956.

15. Ames Research Staff: Equations, Tables, and Charts for Compressible Flow. NACA Rept. 1135, 1953. (Supersedes NACA TN 1428.)

16. Liepmann, H. W.; and Roshko, A.: Elements of Gasdynamics. John Wiley & Sons, Inc., c.1957.

17. Yule, G. Undy; and Kendall, M. G.: An Introduction to the Theory of Statistics. (Available from Hafner Pub. Co., New York.) Fourteenth ed., Charles Griffin & Company Limited (London), c.1958.

18. Beers, Yardley: Introduction to the Theory of Error. Second ed., Addison-Wesley Pub. Co., Inc., 1962.

19. Larson, Terry J.; and Washington, Harold P.: Summary of Rawinsonde Measurements of Temperatures, Pressure Heights, and Winds Above 50,000 Feet Along a Flight-Test Range in the Southwestern United States. NASA TN D-192, 1960.

TABLE I

THERMOCOUPLE SKIN THICKNESS AND FLOW DISTANCE FOR

INSTRUMENTED CHORD OF UPPER VERTICAL FIN

b_w, in.	Blunt leading edge		Sharp leading edge	
	Chord = 8.57 ft		Chord = 9.00 ft	
	x, ft	Percent chord	x, ft	Percent chord
0.037	1.286	15	1.719	19
.037	1.714	20	2.147	24
.037	2.140	25	2.576	29
.037	2.570	30	3.005	33
.030	3.643	42	4.076	45
.030	4.329	50	4.762	53
.030	4.993	58	5.426	60
.030	5.722	66.5	6.205	69
.030	6.408	74.5	6.841	76
.030	7.093	82.5	7.526	84
.030	7.779	90.5	8.212	91

TABLE II

ADDITIONAL CHARACTERISTICS OF BLUNT-LEADING-EDGE

UPPER VERTICAL FIN

Airfoil section	10° single wedge
Total area, sq ft	34.41
Span, ft	4.58
Mean aerodynamic chord, ft	8.95
Root chord, ft	10.21
Tip chord, ft	7.56
Taper ratio	.74
Aspect ratio	.51
Sweep at leading edge, deg	30
Sweep at 25-percent-chord line, deg	23.41
Speed brake total surface area, sq ft	11.18

TABLE III

MEASURED SKIN TEMPERATURES AND FLIGHT CONDITIONS ON BLUNT-LEADING-EDGE VERTICAL FIN

(Flight 2-29)

t, sec	M_∞	p_∞, lb/ft^2	T_∞, °R	α, deg	β, deg	δ, deg	Temperature, °F												
							x, ft												
							Right side						Left side						
							1.286	3.643	4.993	6.408	7.093	7.779	1.286	1.714	2.140	2.570	3.643	4.993	7.779
111	4.15	115	384	4.3	0.38	0.03	660	617	682	634	621	605	660	657	660	630	634	667	662
112	4.16	115	384	4.1	.38	.01	679	633	690	649	625	615	672	670	665	645	651	679	674
113	4.16	115	384	3.9	.38	.01	688	638	697	651	629	620	685	681	674	649	653	685	683
114	4.18	116	383	3.7	.38	.07	690	645	704	656	633	627	684	682	679	651	656	688	682
115	4.19	116	383	3.4	.38	.05	697	647	710	663	645	633	692	692	685	660	665	692	690
[a]116	4.19	117	383	3.3	.38	.01	697	656	715	663	652	636	695	695	690	661	668	695	695
117	4.20	118	383	3.4	.40	.01	709	664	718	673	656	646	704	704	696	667	673	700	704
118	4.21	118	383	3.4	.42	.03	716	671	727	680	666	650	706	709	700	675	680	709	706
119	4.21	119	383	3.0	.42	.03	716	675	725	680	669	652	708	711	702	680	680	711	711
120	4.21	119	383	2.7	.44	.03	716	680	725	687	673	655	709	711	706	682	682	711	718
121	4.22	119	383	2.5	.44	.03	725	684	731	689	675	664	718	718	716	684	687	718	720
122	4.22	120	383	3.2	.42	.03	727	691	736	696	676	664	722	718	716	691	696	720	722
123	4.23	120	383	3.6	.40	.03	737	697	741	697	683	676	726	726	719	697	697	723	732
124	4.23	120	383	3.5	.40	.09	737	699	741	701	694	677	733	733	726	699	699	733	735
125	4.23	120	383	2.9	.52	.13	749	713	753	713	694	682	742	740	735	713	713	740	744
126	4.23	120	383	3.0	.46	.13	746	710	750	715	701	688	743	737	737	710	712	741	743
127	4.24	120	383	3.1	.46	.05	757	717	759	721	701	695	748	748	739	721	717	743	754
128	4.24	120	383	2.9	.48	.03	761	718	761	722	701	696	753	753	742	718	718	744	751
129	4.24	120	383	2.5	.46	.03	770	726	770	728	712	703	764	762	748	726	726	752	759
130	4.24	120	383	4.4	.38	.07	776	734	773	738	712	704	765	765	758	738	734	761	765
131	4.21	120	383	4.7	.42	.07	769	722	765	725	712	704	763	755	751	725	722	751	758
132	4.19	120	383	4.6	.42	-.03	774	737	768	734	719	715	768	768	759	737	737	762	766

[a]Time at which heat-transfer coefficients were reduced for presentation in figure 9.

TABLE III.- Concluded

MEASURED SKIN TEMPERATURES AND FLIGHT CONDITIONS ON BLUNT-LEADING-EDGE VERTICAL FIN

(Flight 2-22)

t, sec	M_∞	p_∞, lb/ft^2	T_∞, °R	α, deg	β, deg	δ, deg	Temperature, °F												
							x, ft												
							Right side						Left side						
							1.286	3.643	4.993	6.408	7.093	7.779	1.286	1.714	2.140	2.570	3.643	4.993	7.779
74	4.80	95	390	1.9	-0.04	-0.35	615	528	626	568	530	533	592	601	586	548	527	600	601
75	4.88	95	390	1.9	.03	-.46	634	550	648	589	544	553	614	628	612	571	545	626	626
76	4.94	94	390	1.6	.07	-.39	663	573	670	611	558	573	636	654	638	602	563	651	651
77	4.98	94	390	1.6	.07	-.46	682	586	692	629	577	593	653	667	655	609	583	676	676
78	5.01	93	390	1.8	.11	-.50	708	604	715	651	598	613	682	686	684	633	595	695	698
79	5.04	93	390	1.7	.03	-.50	718	616	737	664	612	618	694	703	699	644	603	715	715
80	5.07	92	390	1.9	.07	-.50	739	631	757	682	626	636	705	715	708	653	617	724	729
81	5.09	92	390	2.0	.04	-.24	760	651	782	702	647	654	730	741	737	682	638	755	760
82	5.12	92	390	2.0	.19	-.28	778	661	793	715	661	670	750	757	762	703	654	773	782
83	5.14	92	390	1.9	.19	-.31	793	679	816	733	680	686	758	763	765	706	658	785	792
84	5.16	92	390	2.2	.19	-.28	809	690	829	749	698	699	777	790	790	732	682	808	815
85	5.19	92	390	2.2	.21	-.28	820	702	843	760	707	710	787	805	809	748	694	825	834
86	5.21	92	390	2.2	.21	-.28	841	719	864	780	712	724	801	813	819	761	702	840	845
87	5.23	92	390	2.2	.23	-.28	851	731	881	793	719	739	815	826	837	774	722	857	860
88	5.25	92	390	2.3	.19	-.28	855	739	887	806	729	751	833	844	857	795	736	880	880
89	5.26	93	390	2.3	.30	-.28	882	767	912	826	751	765	847	857	867	805	756	889	885
[a]90	5.27	93	390	2.4	.34	-.28	885	771	915	833	765	773	856	870	884	818	775	912	888
91	5.29	93	390	2.8	.44	-.28	902	800	929	849	773	788	867	883	889	826	792	927	893
92	5.30	94	390	2.7	.44	-.28	915	814	949	862	778	802	879	888	899	838	809	937	894
93	5.32	94	390	2.2	.44	-.28	927	829	955	871	797	811	885	899	905	845	827	948	899
94	5.33	95	390	2.2	.44	-.24	940	840	966	881	808	822	902	915	922	857	846	962	902
95	5.33	96	390	2.3	.46	-.28	951	857	978	889	819	831	910	924	928	868	856	973	910
96	5.34	97	390	2.3	.42	-.28	960	869	989	898	827	840	929	938	945	880	873	985	910
97	5.33	98	390	2.4	.42	-.28	962	875	988	900	830	845	936	943	949	891	885	994	911
98	5.33	99	390	2.9	.42	-.28	976	893	1006	915	834	855	941	954	961	901	898	1002	910
99	5.32	100	390	3.8	.48	-.28	982	900	1013	920	837	864	952	962	968	910	904	1000	911

[a]Time at which heat-transfer coefficients were reduced for presentation in figure 9.

TABLE IV

MEASURED SKIN TEMPERATURES AND FLIGHT CONDITIONS ON SHARP-LEADING-EDGE VERTICAL FIN

(Flight 3-23)

t, sec	M_∞,	p_∞, lb/ft^2	T_∞, °R	α, deg	β, deg	δ, deg	Temperature, °F																		
							x, ft																		
							Right side								Left side										
							1.719	2.147	2.576	4.076	4.762	5.426	6.205	8.212	1.719	2.147	3.005	4.076	4.762	5.426	6.205	6.841	7.526	8.212
70	4.24	110	384	1.2	0.2	-0.02	559	539	559	584	531	526	549	554	619	592	566	575	587	566	527	539	518	554
71	4.25	110	384	1.6	.2	-.02	564	550	561	584	542	530	566	559	630	599	570	581	597	570	542	543	533	556
72	4.25	111	384	2.1	.2	-.02	573	561	575	597	551	552	580	573	646	606	581	599	606	577	555	552	549	566
73	4.25	112	384	2.4	.3	.05	581	568	577	600	567	561	593	579	650	619	586	608	619	588	565	568	560	571
74	4.25	111	384	2.1	.3	.05	599	581	595	617	569	570	604	590	663	639	597	617	624	595	576	579	574	581
75	4.26	112	384	2.1	.2	.07	612	595	604	630	587	577	615	601	674	646	606	630	638	601	591	584	587	588
76	4.26	113	384	2.8	.2	.05	619	600	608	642	598	581	626	617	682	650	612	642	649	619	602	602	593	600
77	4.27	112	384	3.7	.2	0	632	617	619	648	604	595	632	626	688	657	622	648	656	630	610	606	604	606
78	4.28	113	384	4.2	.4	-.05	643	621	626	652	621	606	645	630	699	670	632	650	667	641	617	619	604	612
79	4.28	113	384	4.2	.3	0	643	630	639	666	632	612	653	643	716	681	639	663	680	650	630	630	610	628
[a]80	4.28	113	384	4.4	.3	.10	652	641	645	674	634	630	660	648	718	687	645	674	686	656	636	636	617	634
81	4.28	114	384	3.5	.2	.10	663	646	650	681	641	639	667	659	725	697	650	681	697	661	645	639	634	643
82	4.29	115	384	3.2	.3	.02	666	648	661	688	645	644	675	674	732	707	661	688	701	674	653	644	638	650
83	4.29	115	384	3.7	.3	.02	674	657	666	701	660	646	682	677	742	714	674	701	705	679	662	650	643	657
84	4.29	115	384	3.9	.4	0	679	661	674	705	667	650	686	679	749	718	677	705	712	688	665	654	647	661
85	4.30	116	384	3.6	.3	-.43	688	674	681	712	671	654	699	688	755	718	677	712	723	699	669	666	651	670
86	4.31	116	384	3.2	.2	.09	701	679	687	718	678	661	703	703	760	720	687	718	729	707	675	674	660	677
87	4.31	116	384	2.8	.4	.02	709	681	699	722	688	672	712	707	771	722	697	720	733	712	688	677	667	681
88	4.32	117	384	3.1	.4	.02	716	694	707	727	697	677	720	712	778	725	707	727	739	716	688	681	678	685
89	4.33	117	384	3.4	.4	.02	725	699	712	732	705	681	727	718	784	736	716	732	750	718	697	685	680	692
90	4.34	117	384	3.4	.3	0	730	707	716	740	707	688	731	722	784	749	722	740	753	722	701	699	690	701
91	4.34	117	384	3.5	.3	.05	727	714	718	744	707	694	737	725	790	753	732	742	762	732	705	699	690	703
92	4.34	116	384	3.3	.3	.07	738	716	725	749	709	701	744	734	795	755	738	747	774	738	712	709	692	707
93	4.34	116	384	3.3	.4	.10	749	716	732	755	712	707	755	742	801	762	740	755	774	742	718	712	697	712
94	4.35	116	384	3.2	.3	.07	753	718	732	762	718	712	766	747	803	773	742	764	774	742	722	716	707	718
95	4.35	116	384	3.0	.3	.07	760	720	736	762	720	712	768	749	807	778	747	764	779	749	729	718	709	720
96	4.35	117	384	3.0	.4	.07	766	725	740	766	733	716	772	755	813	780	747	766	789	751	737	720	712	725
97	4.35	117	384	3.2	.4	.10	775	736	741	773	738	718	772	755	817	784	749	773	791	762	738	725	720	734
98	4.35	117	384	3.5	.4	.14	775	742	749	778	744	722	772	760	821	786	753	778	796	757	744	729	720	738
99	4.35	117	384	4.0	.4	-.36	780	742	753	780	744	725	774	766	825	788	755	780	802	762	755	734	725	742
100	4.36	116	384	4.0	.5	0	780	747	762	782	755	730	779	766	830	788	760	782	804	764	762	734	725	740
101	4.37	116	384	3.7	.3	0	784	755	766	784	755	732	787	773	834	793	766	784	802	768	766	736	729	744
102	4.37	116	384	3.3	.4	0	784	755	773	788	755	736	787	780	834	788	766	788	802	771	766	736	735	738
103	4.38	115	384	3.1	.4	0	788	762	773	795	764	740	796	780	834	801	767	795	806	773	768	742	738	755
104	4.39	115	384	3.5	.4	0	793	762	773	793	772	749	804	786	832	808	769	795	811	786	772	751	740	758
105	4.40	115	384	3.5	.4	.02	790	764	773	795	772	749	804	786	838	810	778	803	811	786	772	755	744	762
106	4.40	115	384	2.9	.4	.02	795	773	782	790	772	758	804	784	843	815	780	797	806	784	777	755	749	760
107	4.40	114	384	2.7	.4	.10	799	782	790	801	772	764	804	797	856	823	788	808	823	801	779	769	757	775
108	4.39	113	384	3.0	.4	0	799	784	784	799	772	764	804	793	854	825	784	813	825	799	779	766	757	768
109	4.37	113	384	3.1	.4	.05	815	790	797	805	787	762	815	788	858	830	799	817	841	801	789	764	772	768
110	4.35	112	384	3.0	.4	.17	801	786	797	801	779	769	804	797	854	832	790	815	825	799	779	775	759	775

[a]Time at which heat-transfer coefficients were reduced for presentation in figure 9.

TABLE IV.— Concluded

MEASURED SKIN TEMPERATURES AND FLIGHT CONDITIONS ON SHARP-LEADING-EDGE VERTICAL FIN

(Flight 3-31)

t, sec	M_∞	p_∞, lb/ft^2	T_∞, °R	α, deg	β, deg	δ, deg	Temperature, °F																
							x, ft																
							Right side								Left side								
							1.719	2.147	2.576	4.076	4.762	5.426	6.205	8.212	1.719	2.147	3.005	4.076	5.426	6.205	6.841	7.526	8.212
76	5.01	73	401	0.51	0	-0.1	628	612	626	660	599	595	632	597	793	695	653	649	647	617	581	601	597
77	5.06	73	401	.97	0	-.4	649	626	641	683	611	610	651	617	817	721	674	669	667	638	599	614	617
78	5.10	73	401	1.26	0	-.6	670	639	663	706	632	624	670	634	845	745	693	689	691	661	617	632	634
79	5.15	73	401	1.32	0	-.2	688	657	684	725	653	640	698	648	873	766	709	709	712	689	633	651	650
80	5.19	73	401	.72	0	-.2	710	678	704	747	672	658	714	667	901	790	728	730	734	714	651	674	669
81	5.22	73	401	.61	.1	-.2	724	691	721	767	689	674	731	681	924	807	745	750	752	729	670	689	685
82	5.25	73	401	1.39	0	-.1	745	713	742	788	715	691	751	700	949	836	765	769	771	751	693	707	708
83	5.27	73	401	2.65	.2	-.1	763	732	758	812	729	704	768	713	971	853	786	786	786	772	708	727	726
84	5.28	73	401	3.52	.3	-.6	781	749	772	835	747	718	782	731	987	869	804	806	802	788	725	740	739
85	5.29	73	401	2.80	.3	0	796	766	787	852	761	729	795	746	1007	887	822	824	818	801	741	756	757
86	5.30	73	401	2.06	.3	0	815	778	803	873	778	740	808	761	1023	905	841	841	834	819	758	773	769
[a]87	5.31	74	401	1.98	.2	0	827	788	812	886	795	752	825	771	1036	917	851	853	847	838	775	793	782
88	5.33	74	400	2.53	.2	0	842	802	829	906	810	766	836	787	1050	936	869	867	862	853	796	812	796
89	5.34	75	400	3.07	.3	0	854	813	842	921	822	777	852	798	1064	946	875	882	871	869	809	820	806
90	5.36	75	400	3.47	.3	.1	869	829	854	935	836	781	866	809	1079	959	892	892	882	885	820	832	816
91	5.37	75	400	3.62	.3	-.1	881	840	868	947	849	796	876	820	1088	968	908	902	893	902	835	843	831
92	5.38	75	400	3.47	.3	-.1	890	852	878	966	862	809	884	833	1094	977	919	914	904	911	850	856	844
93	5.38	75	400	2.84	.3	-.1	900	860	884	979	873	818	898	842	1102	981	929	918	912	924	856	862	852
94	5.37	75	400	2.78	.2	-.1	911	869	897	989	892	831	911	854	1109	995	938	929	927	942	869	873	860
95	5.35	76	400	3.09	.2	-.2	920	880	909	997	902	838	914	861	1119	1005	948	935	939	947	880	881	866
96	5.33	76	400	3.01	.3	-.2	932	886	917	1004	907	847	920	869	1125	1012	956	944	946	949	886	896	875
97	5.28	76	400	3.43	.3	.2	940	896	926	1010	913	853	924	875	1130	1019	963	950	952	953	896	901	882
98	5.23	76	400	3.16	.3	.2	949	910	941	1015	919	863	929	881	1136	1026	975	958	958	957	904	912	889

[a]Time at which heat-transfer coefficients were reduced for presentation in figure 9.

TABLE V

MEASURED LOCAL STATIC PRESSURES ON SHARP-LEADING-EDGE VERTICAL FIN

Flight 3-23, M = 4.2

t, sec	M_∞	Pressure, lb/ft^2					
		x, ft					
		0.720	0.990	2.61	2.970	4.950	6.300
70	4.24	180	170	195	202	140	125
75	4.26	185	177	195	205	135	125
80	4.28	188	175	200	210	135	132
85	4.30	190	185	200	210	135	135
90	4.34	188	180	205	212	130	135
95	4.35	186	182	202	215	135	135
100	4.36	192	178	200	210	132	135
105	4.40	198	180	200	207	132	130
110	4.35	186	172	190	200	128	128

Flight 3-31, M = 5.3

t, sec	M_∞	Pressure, lb/ft^2					
		x, ft					
		0.720	0.990	2.61	2.970	4.950	6.300
76	5.01	130	124	144	143	100	85
81	5.22	132	122	152	145	98	85
86	5.30	126	119	137	137	89	82
91	5.37	126	120	134	131	81	85
96	5.33	129	120	142	135	81	86
101	----	127	119	141	128	81	84

TABLE VI

MEASURED LOCAL STATIC PRESSURES ON BLUNT-LEADING-EDGE VERTICAL FIN

Flight 2-29, M = 4.2

t, sec	M_∞	Pressure, lb/ft^2					
		x, ft					
		0.514	1.286	2.142	4.456	5.828	7.199
105	4.09	188	175	210	162	178	170
110	4.14	195	185	200	162	180	182
115	4.19	200	175	210	165	175	168
120	4.21	205	190	218	175	187	185
125	4.23	208	188	210	168	185	185
130	4.24	200	185	210	168	192	168
135	4.10	192	178	198	152	172	160

Flight 2-22, M = 5.3

t, sec	M_∞	Pressure, lb/ft^2					
		x, ft					
		0.514	1.286	2.142	4.456	5.828	7.199
71	4.63	105	82	105	65	83	92
76	4.94	150	130	140	100	130	130
81	5.09	190	170	190	150	180	170
86	5.21	197	155	185	155	195	175
91	5.29	210	150	180	160	200	180
96	5.34	222	145	180	160	210	185
101	5.29	225	140	190	165	215	195

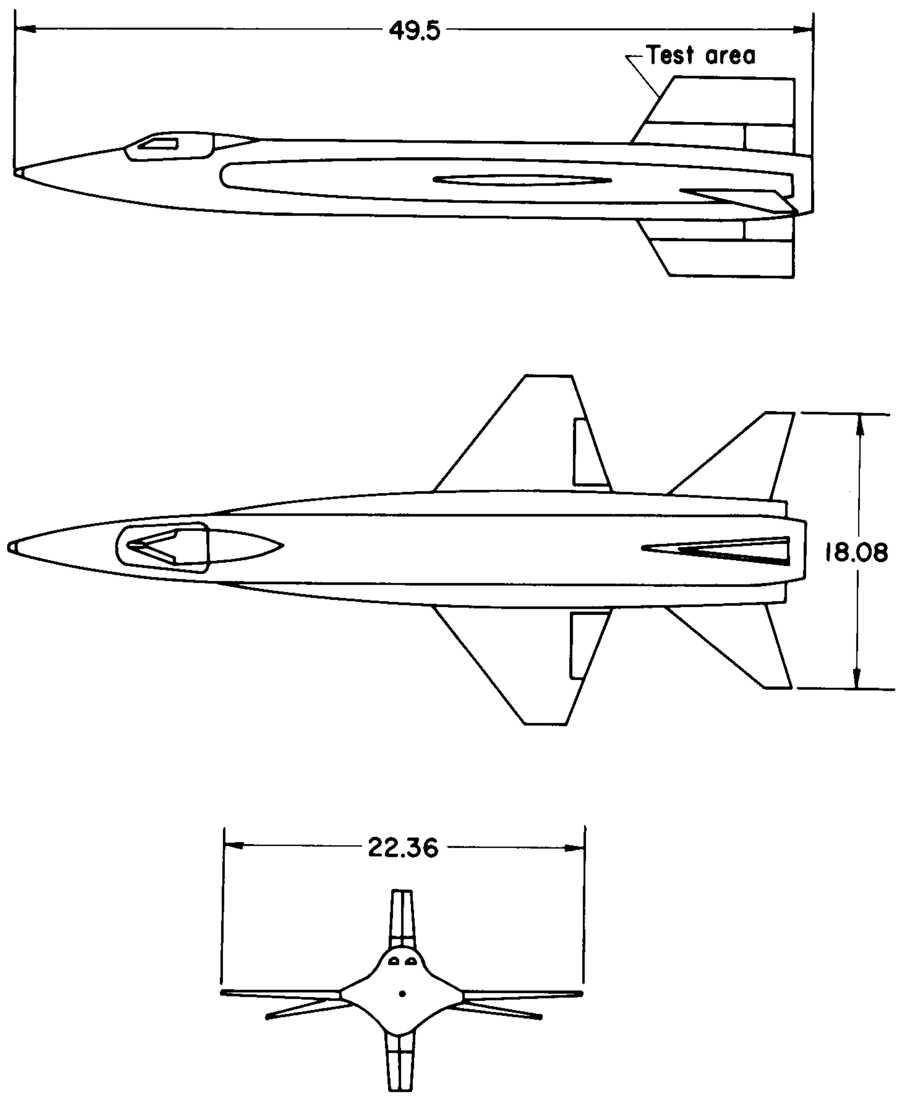

Figure 1.– Three-view drawing of the X-15 research airplane.

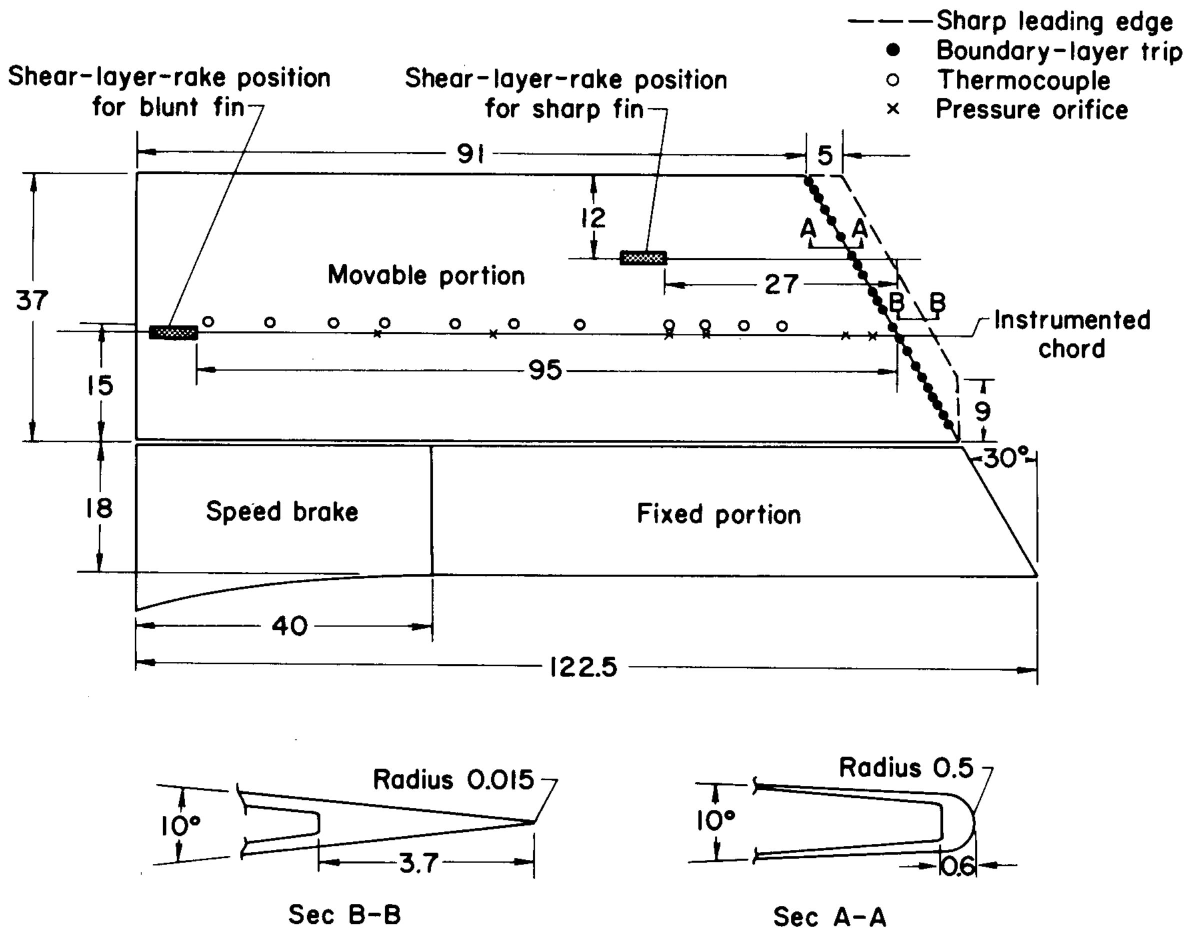

Figure 2.- Sketch of X-15 upper vertical fin showing instrumentation. All dimensions in inches unless noted.

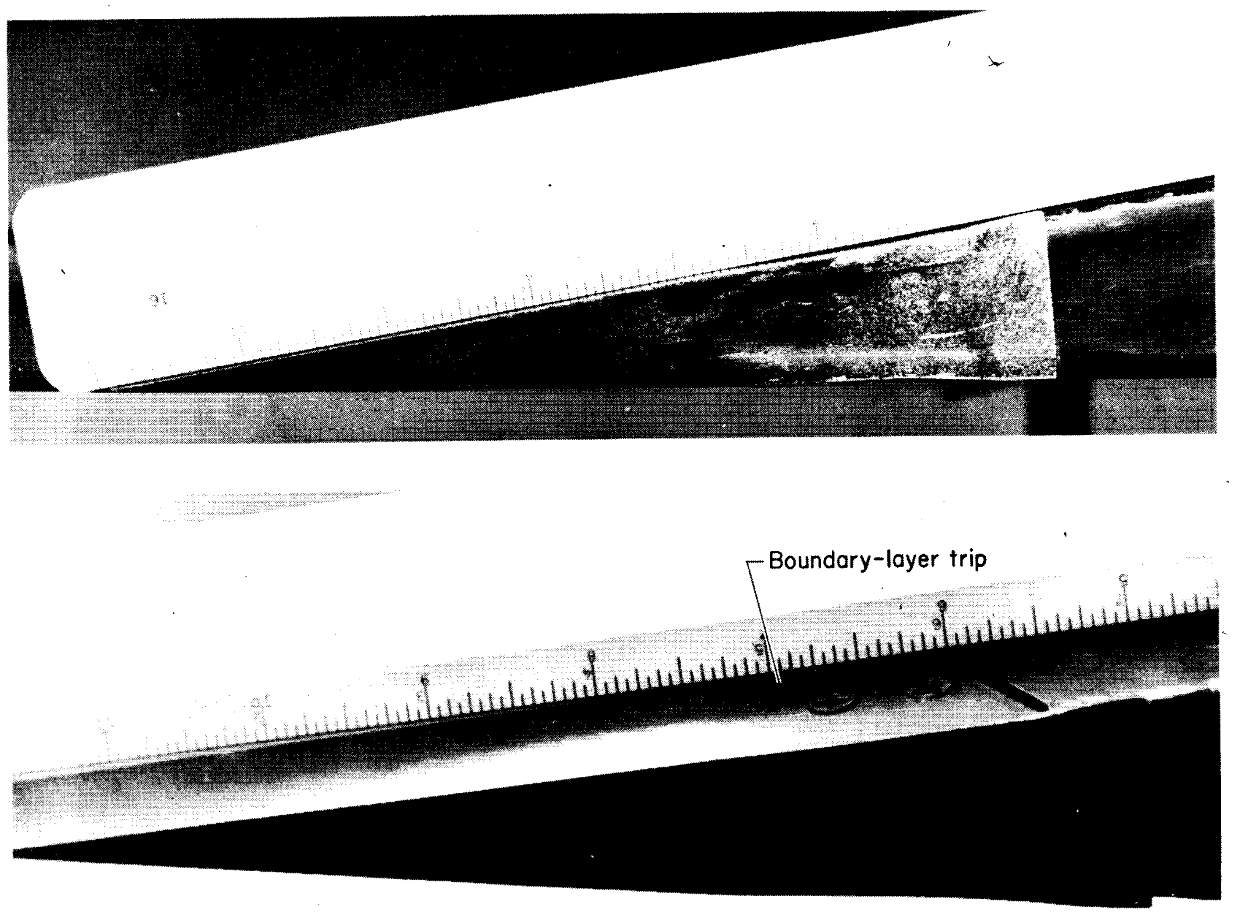

Figure 3.- Edge view of sharp-leading edge and a boundary-layer trip.

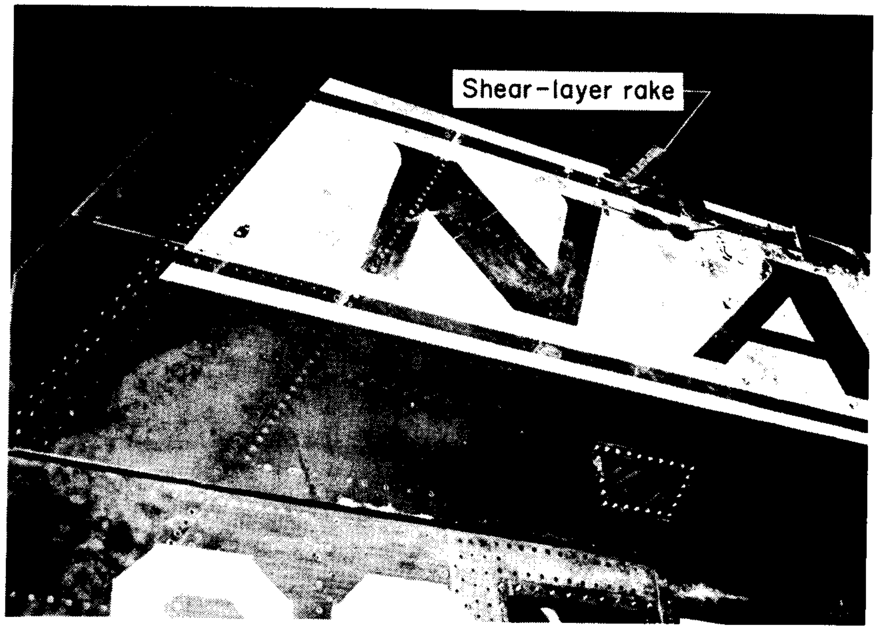

(a) Sharp fin.

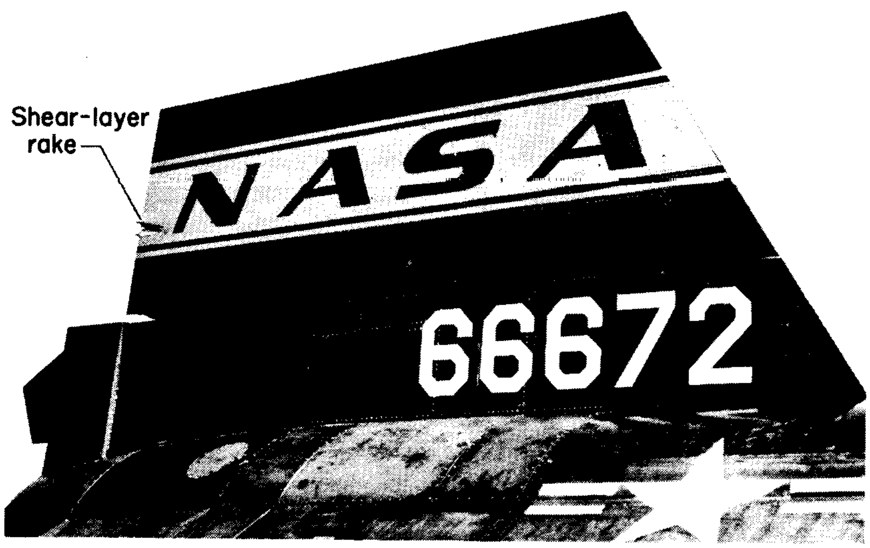

(b) Blunt fin.

Figure 4.— Photos of shear-layer rake on sharp- and blunt-leading-edge fins.

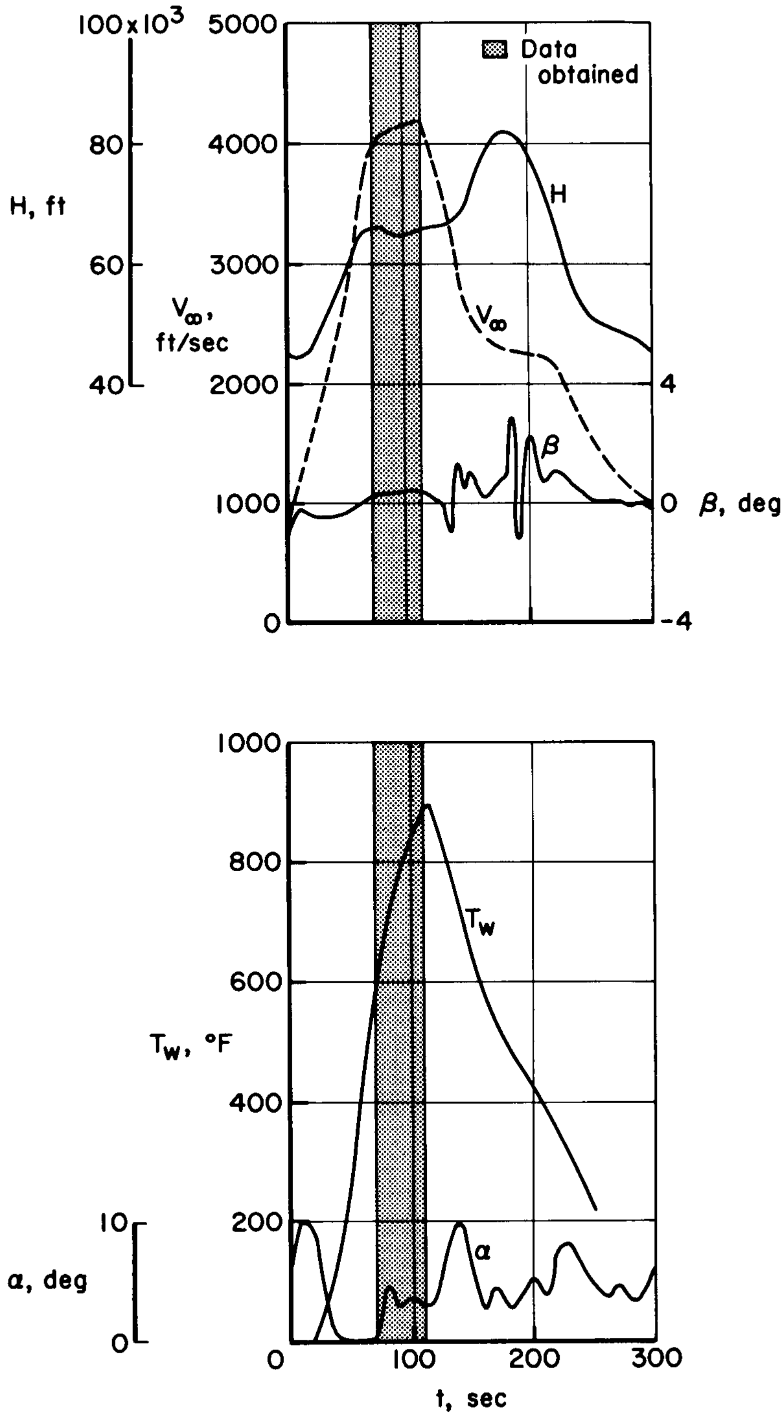

Figure 5.- Time history of typical heating flight (3-23).

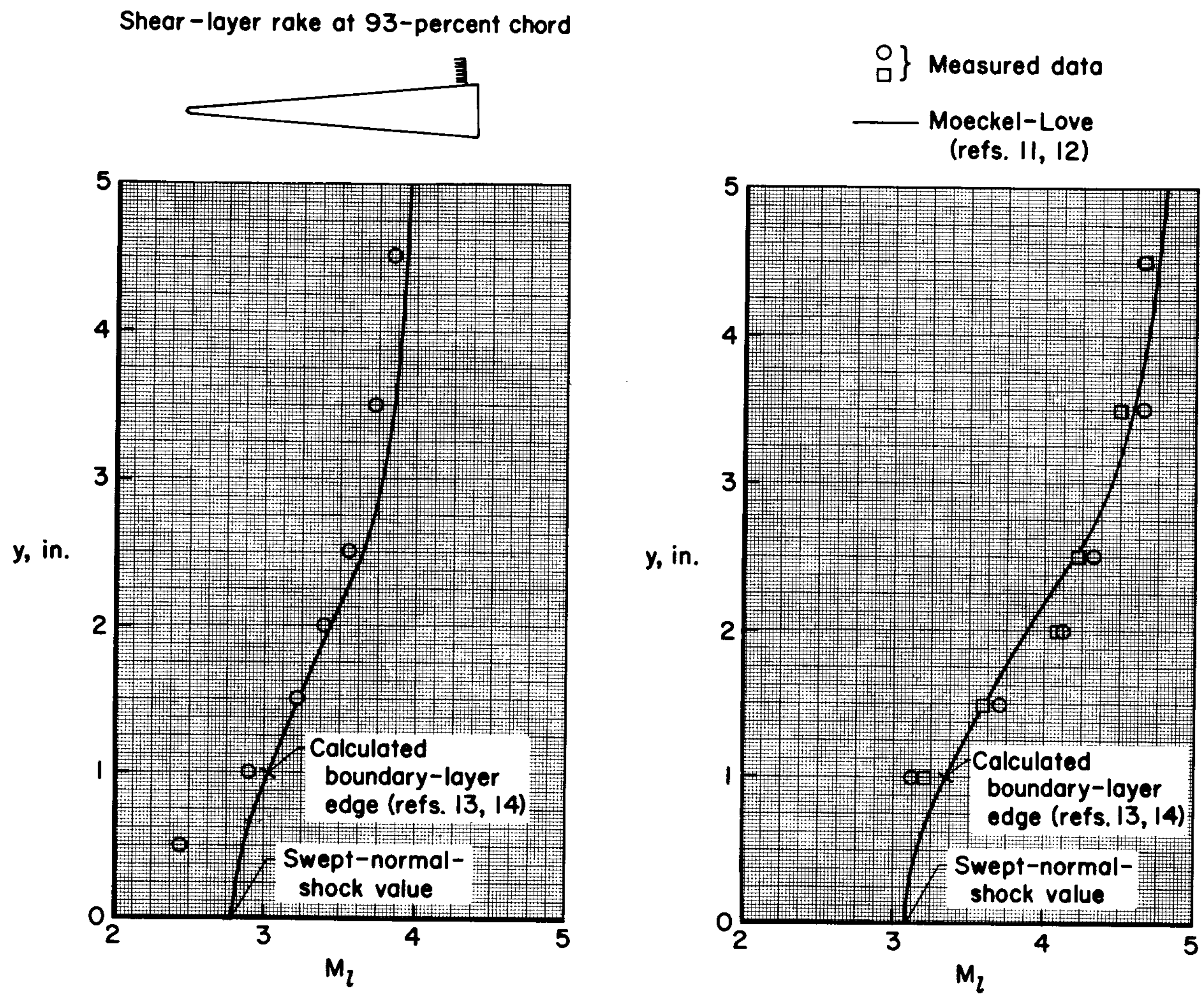

(a) $M_\infty = 4.2, \quad \frac{p_l}{p_\infty} = 1.35.$

(b) $M_\infty = 5.1, \quad \frac{p_l}{p_\infty} = 1.35.$

Figure 6.– Measured and calculated shear-layer profiles for the blunt fin.

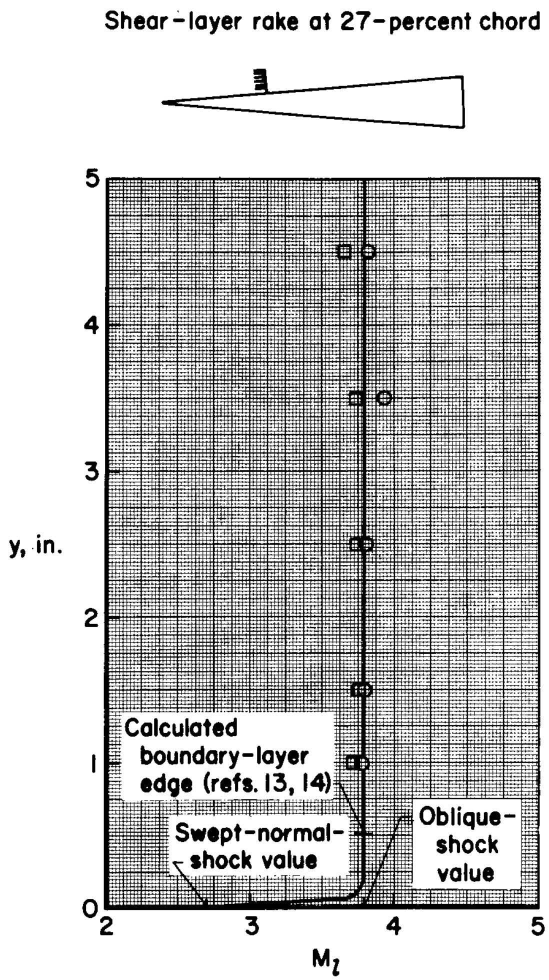

(a) $M_\infty = 4.2$, $\frac{p_l}{p_\infty} = 1.60$.

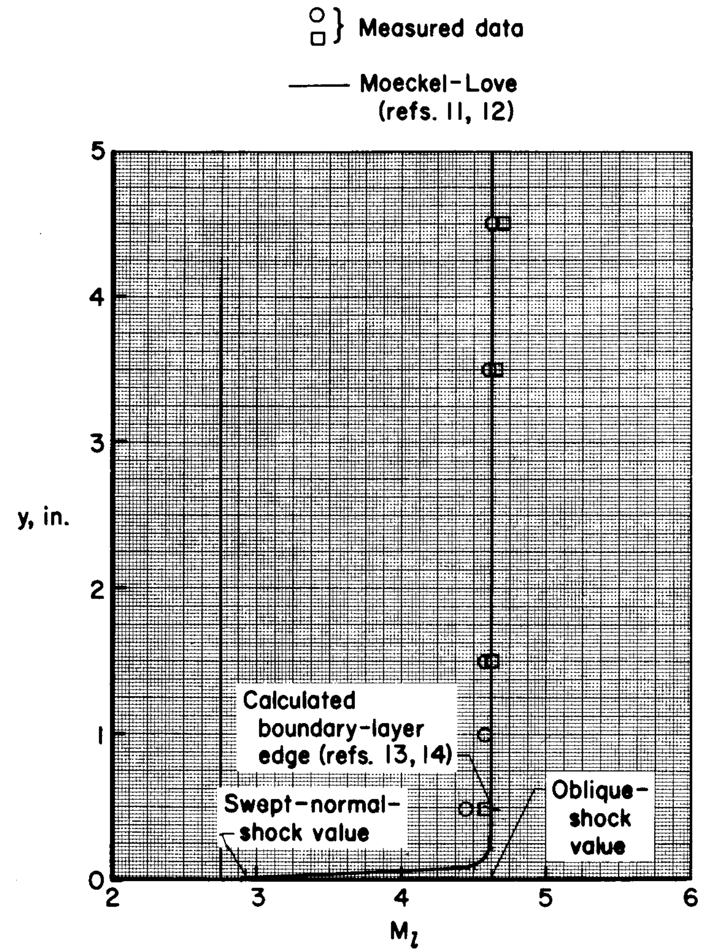

(b) $M_\infty = 5.1$, $\frac{p_l}{p_\infty} = 1.76$.

Figure 7.- Measured and calculated shear-layer profiles for the sharp fin.

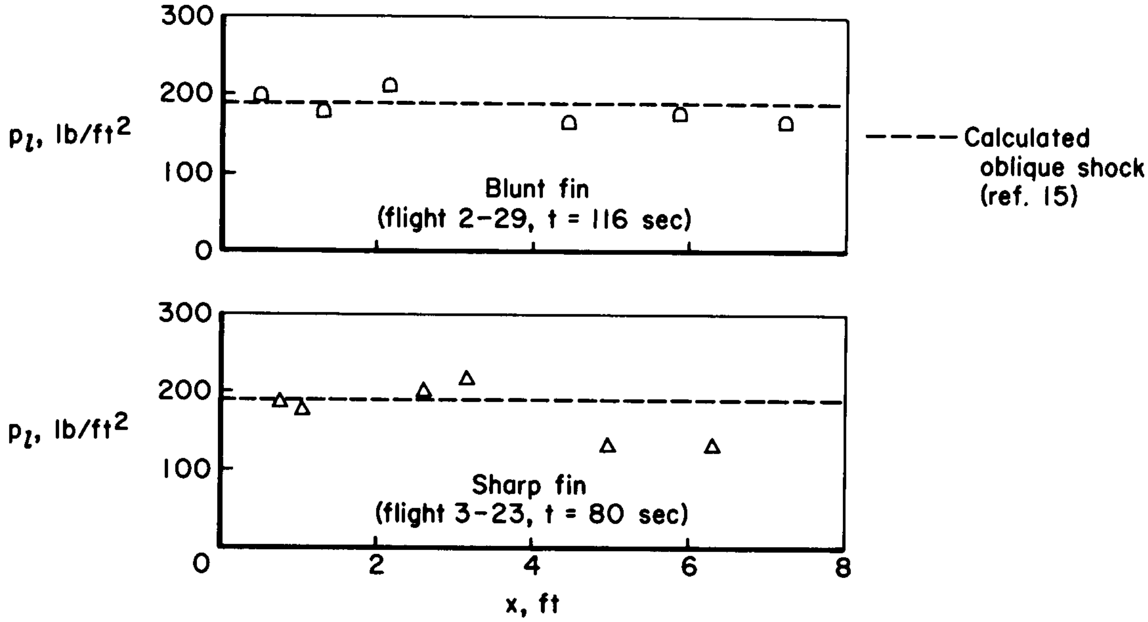

(a) $M_\infty = 4.2$.

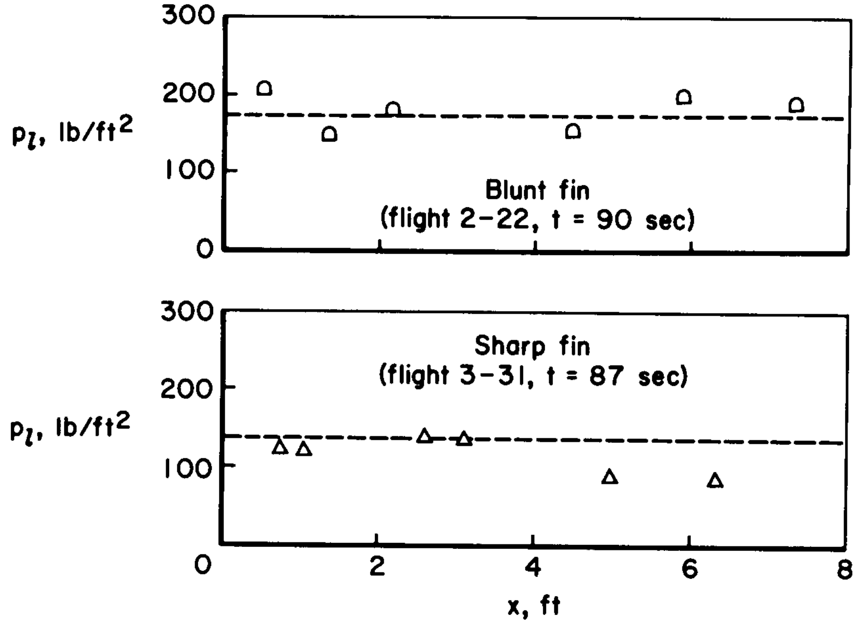

(b) $M_\infty = 5.3$.

Figure 8.- Comparison of measured and calculated local static pressure on the surface of the sharp and the blunt vertical fin.

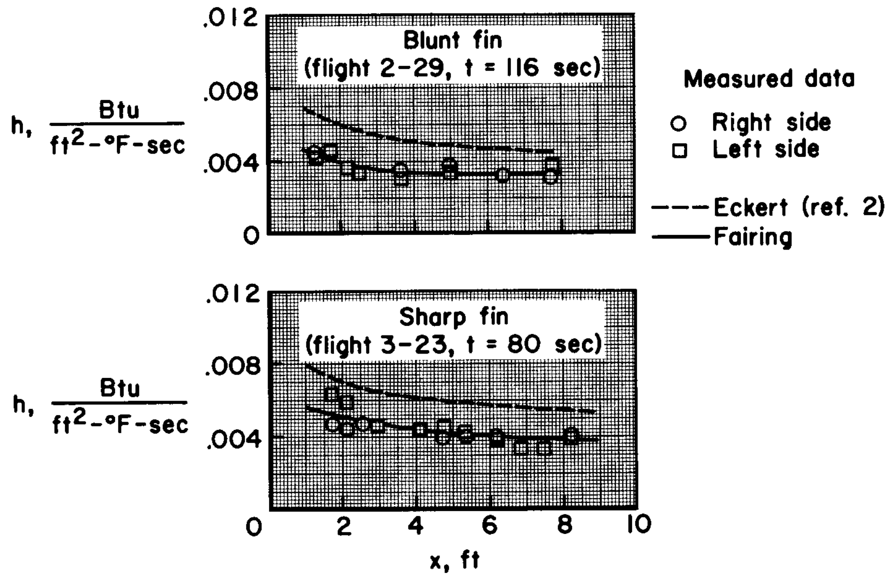

(a) $M_\infty = 4.2$.

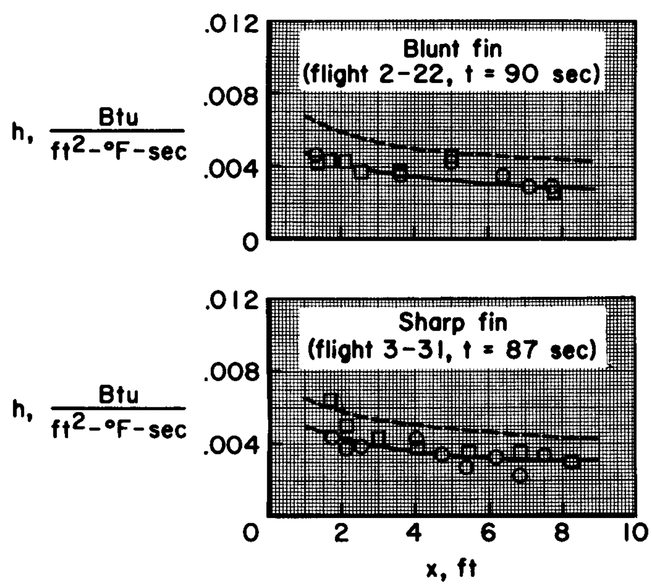

(b) $M_\infty = 5.3$.

Figure 9.— Comparisons of measured and calculated turbulent heat-transfer coefficients on the sharp and the blunt vertical fin.

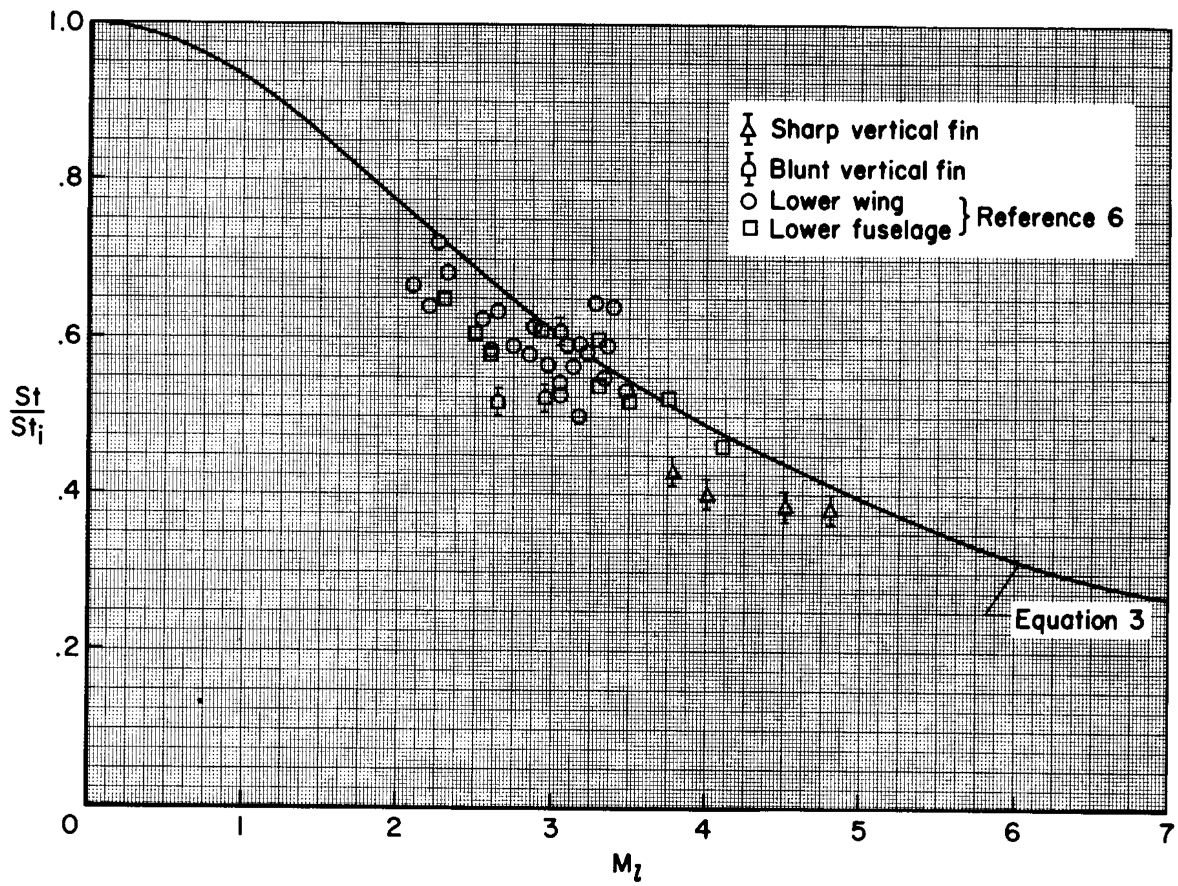

Figure 10.— Comparison of measured and calculated heat-transfer coefficients from various X-15 surfaces.

NASA-Langley, 1965 H-382